



UNIVERSITÀ DI PARMA

ARCHIVIO DELLA RICERCA

University of Parma Research Repository

Strain Field Self-Diagnostic Poly(dimethylsiloxane) Elastomers

This is the peer reviewed version of the following article:

Original

Strain Field Self-Diagnostic Poly(dimethylsiloxane) Elastomers / Fruh, Andreas Enrico; Artoni, Federico; Brighenti, Roberto; Dalcanale, Enrico. - In: CHEMISTRY OF MATERIALS. - ISSN 0897-4756. - 29:17(2017), pp. 7450-7457. [[10.1021/acs.chemmater.7b02438](https://doi.org/10.1021/acs.chemmater.7b02438)]

Availability:

This version is available at: 11381/2829762 since: 2021-09-29T12:42:48Z

Publisher:

American Chemical Society

Published

DOI:[10.1021/acs.chemmater.7b02438](https://doi.org/10.1021/acs.chemmater.7b02438)

Terms of use:

Anyone can freely access the full text of works made available as "Open Access". Works made available


Publisher copyright

note finali coverpage

(Article begins on next page)

24 April 2024

Strain Field Self-Diagnostic Poly(dimethylsiloxane) Elastomers

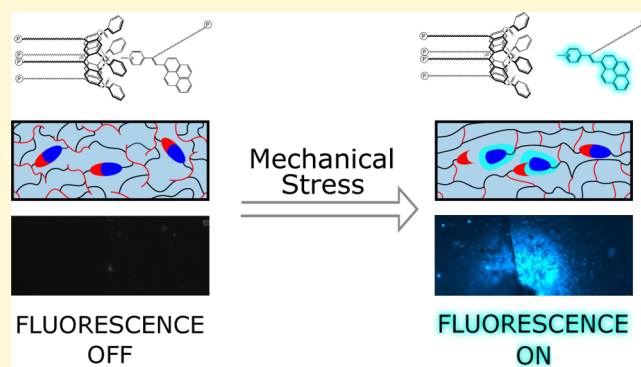
Andreas E. Früh,[†] Federico Artoni,[‡] Roberto Brighenti,^{*,‡} and Enrico Dalcanale^{*,†} 

[†]Department of Chemistry, Life science and Environmental Sustainability, University of Parma and INSTM UdR Parma, Parco Area delle Scienze 17/A, 43124 Parma, Italy

[‡]Department of Engineering & Architecture, University of Parma, Parco Area delle Scienze 181/A, 43100 Parma, Italy

Supporting Information

ABSTRACT: Advanced applications, involving high risk mechanical systems, require the in-service deformation level to be verified in order to assess their safety and reliability, providing information for repairing or replacing interventions. In the present work, a self-diagnostic poly(dimethylsiloxane) (PDMS) elastomer containing a supramolecular detection probe is proposed, enabling the strain intensity in the polymeric matrix to be identified by fluorescence detection. Turn-on fluorescence represents an efficient, sensitive, simple, and real time diagnostic tool to quantitatively detect high-strain regions for the mechanical monitoring of structural elements. The supramolecular complex—cross-linking the polymer's chains—provides fluorescence response induced by strain even if present in a very low amount (10^{-6} mol kg⁻¹), completely preserving the mechanical characteristics of the matrix. The developed PDMS material is mechanically tested, and the observed fluorescence field is correlated with that obtained by numerical simulations as well as by contactless measurements performed via the digital image correlation (DIC) technique.



INTRODUCTION

Polymers are desirable materials for high-performance applications, due to their affordable price, light weight, and processability. However, small damages, which are difficult to detect, can compromise the mechanical integrity of the material and subsequently lead to failure. Molecular probes are ideal candidates to facilitate the detection of such damages and thus to prevent catastrophic failure, visualizing mechanical strain and/or damage as an easily detectable alert signal at a very early stage. A range of mechanochemical reporters, based on force induced redistributions of a chemical equilibrium, have been published,^{1–6} including spiropyran-^{7–10} and dioxetane-^{11–14} based systems. Other systems are based on physical effects such as aggregation or separation-induced emission,^{15,16} alteration of the band gap by physical deformation of SWCNT,^{17,18} or mechanochromism.^{19–21} However, those probes have the drawback that relatively large quantities of the active system are needed, which alters the mechanical properties of the polymer and significantly increases the price of the material. Probes based on the force induced redistributions of a chemical equilibrium add covalent cross-links to the system. Systems based on physical effects, like the aggregation or separation-induced emission, are relatively sensitive, but they need specially engineered polymers, in the form of solvent-filled microcapsules or the layering of different materials. PDMS elastomers are among the polymeric matrices used to detect mechanical damage with mechanophores.²² In a step forward, Sijbesma et al. reported a strain-field sensitive mechanolumi-

nescent PDMS elastomer equipped with dioxetane cross-linkers, capable of reporting “mechanomemory” effects in the polymer.²³

In hydrostatic stress-sensitive materials containing microvoids or microdefects, the knowledge of the volumetric strain is fundamental for their safety level assessment yet demanding to determine in service.^{24,25} The volumetric strain physically corresponds to the mean strain value, obtained by averaging the strain components with respect to all the 3D space directions.²⁶ In such materials, the presence of a tensile hydrostatic stress state can lead to an expansion and coalescence of microvoids and inclusions (often identified as cavitation-like failure), triggering the subsequent crack appearance and growth.²⁷

The above-described mechanism becomes much more relevant in the case of materials withstanding repeated loads (fatigue). The capability to monitor the maximum volumetric strain occurring in the element under service enables its design to be optimized and the safety level to be enhanced. The direct measure of the average strain is not feasible, and the determination of the volumetric strain requires strain measurements in multiple directions, an operation that can be prohibitive in small or thin elements. A possible solution is adding a probe capable of detecting and reporting mechanical deformations at the molecular level. The availability of a

Received: June 12, 2017

Revised: July 31, 2017

Published: July 31, 2017

76 molecular-based detection tool is highly desirable to map highly
77 volumetric strained regions without the need of any complex
78 measurement device and without affecting the microstructure
79 bearing capability of the material. Further, self-diagnostic
80 capability allowed by molecular interactions (i.e., at the
81 nanoscale level) entails no restrictions on the scale of the
82 element to be analyzed and opens the way to the monitoring of
83 objects of any size.

84 In this paper, we introduce a self-diagnostic PDMS elastomer
85 containing a supramolecular detection probe, which is able to
86 report areas of high strain in the polymeric matrix by
87 fluorescence turn-on. Turn-on fluorescence, which is easily
88 detectable with suitable equipment, offers an excellent contrast
89 between high-strain affected and unaffected regions, providing a
90 very sensitive tool for the monitoring of structural elements.

91 ■ EXPERIMENTAL SECTION

92 **Synthesis.** 4-(Dodec-11-en-1-yl)pyridine. 4-Picoline (2.6 mL,
93 29.17 mmol) was dissolved in dry THF (12 mL), and the solution
94 was cooled to $-41\text{ }^{\circ}\text{C}$ with an acetonitrile–liquid nitrogen slush
95 bath.²⁸ *n*-Butyllithium in hexanes (2.5 M, 13.5 mL, 33.75 mmol) was
96 added over 30 min. The reaction was stirred for an additional 5 min at
97 $-41\text{ }^{\circ}\text{C}$, and then the bath was removed and the reaction allowed to
98 warm up to room temperature. After 1 h, additional dry THF (12 mL)
99 was added to dilute the 4-picolylithium slurry and the obtained
100 solution stirred for 1 h more. The solution was cooled with an ice bath
101 to $0\text{ }^{\circ}\text{C}$ and added over 30 min into a solution of 11-bromo-1-
102 undecene (7.0 mL, 31.91 mmol) in THF (5.0 mL) at $-41\text{ }^{\circ}\text{C}$. The
103 reaction was allowed to warm up to room temperature and stirred for
104 21 h. Water (1.5 mL) was added, the obtained mixture filtered over a
105 silica pad, and the pad washed with ethyl acetate ($6 \times 30\text{ mL}$). The
106 organic phases were combined, the solvent removed, and the residue
107 further purified by flash chromatography (Hex/EtOAc 1.5/1), yielding
108 a yellow oil (4.15 g, 50% yield). ¹H NMR (300 MHz, CDCl₃) δ : 8.42
109 (d, $J = 6.0\text{ Hz}$, 2H, α Py H), 7.03 (d, $J = 5.5\text{ Hz}$, 2H, β Py H), 5.75
110 (ddt, $J = 17.0, 10.3, 6.7\text{ Hz}$, 1H, CH=CH₂), 4.97–4.85 (m, 2H,
111 CH=CH₂), 2.53 (t, $J = 7.7\text{ Hz}$, 2H, Py-CH₂), 1.98 (q, $J = 7.0\text{ Hz}$,
112 2H, CH₂-CH=CH₂), 1.55 (q, $J = 7.3\text{ Hz}$, 2H, Py-CH₂-CH₂),
113 1.34–1.22 (m, 15H). ¹³C NMR (75 MHz, CDCl₃, δ): 151.5 (γ Ar C),
114 149.5 (α Py C), 139.0 (CH=CH₂), 123.8 (β Py C), 114.1 (CH=
115 CH₂), 35.2 (Py-CH₂), 33.7 (CH₂-CH=CH₂), 30.2, 29.50, 29.44,
116 29.42, 29.34, 29.12, 29.07, 28.87. MS (ESI) m/z : [M + H]⁺ calcd for
117 C₁₇H₂₈N, 246.22; found, 246.28.

118 *N*-Methyl-4-(dodec-11-en-1-yl)pyridinium iodide. 4-(Dodec-11-
119 en-1-yl)pyridine (561 mg, 2.29 mmol) was dissolved in iodomethane
120 (4.0 mL, 46.3 mmol) and refluxed under nitrogen for 6 h. The product
121 was precipitated with diethyl ether, filtered off, washed with diethyl
122 ether, and dried in vacuo, yielding an off-white solid (884 mg, 100%).
123 ¹H NMR (300 MHz, CDCl₃) δ : 9.24 (d, $J = 6.6\text{ Hz}$, 2H, α Py H),
124 7.84–7.80 (m, 2H, β Py H), 5.87–5.71 (m, 1H, CH=CH₂), 5.01–
125 4.84 (m, 2H, CH=CH₂), 4.63 (s, 3H, N-CH₃), 2.90–2.81 (m, 2H,
126 Py-CH₂), 2.06–1.94 (m, 2H, CH₂-CH=CH₂), 1.74–1.60 (m, 2H,
127 Py-CH₂-CH₂), 1.32–1.18 (m, 15H). MS (ESI) m/z : [M – Iodine]⁺
128 calcd for C₁₈H₃₀N, 260.24; found, 260.27.

129 *N*-Methyl-4-(1-(pyren-1-yl)trideca-1,12-dien-2-yl) Pyridinium Iodide
130 (Guest). 1-Pyrenecarboxaldehyde (400 mg, 1.74 mmol) was
131 dissolved in ethanol (3.0 mL), and *N*-methyl-4-(dodec-11-en-1-
132 yl)pyridinium iodide (236 mg, 0.61 mmol) and piperidine (200 μL)
133 were added. The reaction was stirred under reflux for 16 h, then the
134 solvent removed, and the obtained crude purified by flash
135 chromatography (DCM/MeOH 95/5), yielding an orange solid (44
136 mg, 12%). ¹H NMR (300 MHz, CDCl₃) δ : 9.27 (d, $J = 6.7\text{ Hz}$, 2H, α
137 Py H), 8.82 (d, $J = 6.7\text{ Hz}$, 2H, β Py H), 8.23–7.96 (m, 8H, Pyrene),
138 7.56 (d, 1H, H(10)–Pyrene), 5.83–5.72 (m, 1H, CH=C), 5.05–4.90
139 (m, 1H), 4.70 (s, 3H, N-CH₃), 2.89–2.71 (m, 2H, Py-CH₂), 2.06–
140 1.94 (m, 2H, CH₂-CH=CH₂), 1.64–1.60 (m, 2H, Py-CH₂-CH₂),
141 1.44–1.04 (m, 15H). MS (ESI) m/z : [M – I]⁺ calcd for C₃₅H₃₈N,
142 472.30; found, 472.34.

Tetraphosphonate Cavitand Host. The host was prepared 143
514 according to a published procedure.^{29,30}

PDMS Preparation. A commercially available room temperature 145
vulcanization silicone kit, RTV 615 (Momentive Performance 146
Materials Inc., Waterford, NY) was used to prepare the matrix. 147

Dichloromethane solution of guest ($c = 10^{-5}\text{ M}$) and host ($c = 2 \times$ 148
 10^{-5} M) were prepared in order to form the supramolecular complex 149
and to easily measure the desired quantities. The required quantities of 150
the solutions or a mixture thereof was added to component A of RTV 151
615 and the solvent subsequently removed by warming the 152
component to $60\text{ }^{\circ}\text{C}$. Mixing of the preloaded component A with 153
component B and subsequent curing at $40\text{ }^{\circ}\text{C}$ overnight yielded the 154
used polymer samples. 155

Fluorescence Characterization. Samples for fluorescence 156
characterization were prepared using the required amount of guest 157
solution with or without an equivolumar amount host solution in 158
order to obtain samples with a concentration of $b(\text{guest}) = 10^{-6}\text{ mol}$ 159
 kg^{-1} . Preparation was performed as described above, and the obtained 160
samples were cured at $40\text{ }^{\circ}\text{C}$ overnight directly in cuvettes 161
(poly(methyl methacrylate), path length 10 mm, Sigma-Aldrich 162
Z188018). Spectra were recorded on a PerkinElmer LS 55 163
Fluorescence spectrometer using FL WinLab.³¹ Data was plotted 164
using gnuplot.³² 165

Stress Test Samples. Samples for mechanical stress tests were 166
prepared using the required amount of guest solution mixed with an 167
equivolumar amount of host solution in order to obtain samples with a 168
concentration of $b(\text{guest}) = 10^{-6}\text{ mol kg}^{-1}$. Blank samples were 169
prepared without any additions. Samples were cured in a custom-made 170
aluminum mold, yielding specimens with the dimensions shown in 171
Figure 8. 172

The obtained precracked samples were mechanically tested under a 173
three-point bending system; a vertical controlled downward displace- 174
ment δ was applied to the top central point of the beam at a rate equal 175
to about $\delta = 5 \times 10^{-5}\text{ m s}^{-1}$; the corresponding restraint force F (see 176
Figure 8a) was measured during the test. The applied displacement δ 177
was increased until the crack started growing upward (leading roughly 178
to the development of a crack nearly along the middle cross-section of 179
the beam specimen; see Figure 10) and continuously increased until 180
the crack reached a final length equal to about 3 times its initial size 181
before the final failure of the specimen. Besides mechanical and 182
kinematic measurements, the specimens were also monitored through 183
the Digital Image Correlation (DIC) technique to quantitatively 184
measure the displacement and the strain field of the surface of the 185
specimen. 186

High resolution pictures were taken for some increments of the 187
applied displacement at a step equal to $\Delta\delta = 5 \times 10^{-4}\text{ m}$ and 188
processed through the freely available DIC analyzer Ncorr 189
software.^{33,34} 190

After the mechanical test, the samples were examined using a Nikon 191
Eclipse Ti (Nikon Corp., Tokyo, Japan) equipped with a UV-1A 192
ultraviolet excitation filter block (Nikon Corp., Tokyo, Japan); 193
excitation filter wavelengths: 360–370 nm (bandpass, 365 CWL); 194
dichromatic mirror cut-on wavelength: 380 nm (long-pass, LP); 195
barrier filter wavelengths: 420 nm cut-on (long-pass, LP)) and an 196
Andor Clara Interline CCD camera (Oxford Instruments, U.K.). 197
Pictures were taken and processed using ImageJ.³⁵ 198

199 ■ RESULTS AND DISCUSSION

The working mechanism of the proposed stress self-diagnostic 200
polymeric system is sketched in Figure 1. Its operation is based 201
on the introduction of a tiny amount of fluorescence silent 202
host–guest complexes in the polymer matrix as supramolecular 203
cross-links, which break apart upon mechanical stress in the 204
strained zone leading to localized fluorescence emission. 205

Since host–guest interactions are considerably weaker than 206
covalent bonds, the disconnection of the supramolecular cross- 207
links takes place well before the covalent bonds are broken, 208
providing an early signal that the mechanical integrity of the 209

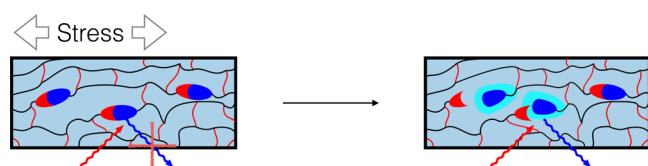


Figure 1. Schematic representation of the self-diagnostic polymer working system.

210 polymer is compromised. Very small quantities of the reporting
211 system are needed; therefore, the physical and mechanical
212 properties of the resulting self-diagnostic polymer are not
213 altered.

214 **Design and Synthesis of the Host–Guest Reporting**
215 **Probe and Preparation of the Corresponding PDMS.** The
216 chosen host–guest complex, shown in Figure 2, consists of a
217 tetraphosphonate cavitand as host and an *N*-methylated
218 pyridinium salt as guest. Both the guest and the host are
219 functionalized with terminal double bonds (one in the case of
220 the guest, four in the case of the host), over which the complex
221 is randomly incorporated into the PDMS matrix, thereby
222 adding supramolecular cross-links to the system.

223 Tetraphosphonate cavitands are versatile molecular receptors
224 capable of binding *N*-methylpyridinium³⁶ and *N*-methylammo-
225 nium salts with remarkable selectivity.³⁷ Tetraphosphonate
226 cavitands form highly stable complexes with *N*-methylpyr-
227 idinium salts in apolar environments ($K_a = 5.8 \times 10^6 \text{ M}^{-1}$ in
228 1,2-dichloroethane)³⁸ via synergistic cation–dipole interactions
229 between the charged nitrogen and the P=O groups and
230 cation– π interactions between the methyl group and the π -
231 basic cavity.³⁹ The guest design is inspired by another system
232 reported in the literature,⁴⁰ which uses the quenching of a

233 similar guest consisting of an *N*-methylated pyridinium
234 conjugated to a pyrene in combination with calix[*n*]arene-*p*-
235 sulfonates as the artificial acetylcholine detection system.

236 The incorporation strategy requires the insertion of the
237 reporting system as the preformed complex in the polymer
238 precursors before polymerization, to have complete fluores-
239 cence quenching of all guests before mechanical tests.
240 Moreover, the complex must be indefinitely stable in the
241 unstressed polymer. The polymeric matrix compatible with the
242 host–guest complex is a commercial RTV silicone rubber
243 (poly(dimethylsiloxane), PDMS), obtained by the platinum
244 catalyzed reaction of a vinyl PDMS prepolymer with a silicon
245 hydride component (H-PDMS, Figure 3), via formation of
246 ethyl cross-linking bridges between the two.⁴¹

247 To incorporate the host–guest complex into the polymer
248 matrix, both the host and the guest are functionalized with ω -
249 alkenyl chains. The terminal double bonds are able to react
250 during the curing of the used PDMS system, inserting the
251 reporting complex randomly into the PDMS matrix. The
252 alkenyl chains are long enough to permit sufficient conforma-
253 tional flexibility to the complex to avoid its mechanical
254 dissociation during the curing of the matrix. The preformed
255 complex is soluble and stable in the PDMS matrix.

256 The synthesis of the tetraphosphonate cavitand bearing four
257 ω -undecenyl chains is described in the literature.^{29,30}
258 Preparation of the guest was performed starting from 4-
259 picoline, which was first alkylated with the double bond
260 terminated linker chain in the benzylic position using *n*-
261 butyllithium. The obtained pyridine was subsequently methy-
262 lated using iodomethane and the obtained pyridinium salt
263 condensed with 1-pyrenecarboxaldehyde in a Knoevenagel
264 condensation, yielding the desired guest molecule. The host

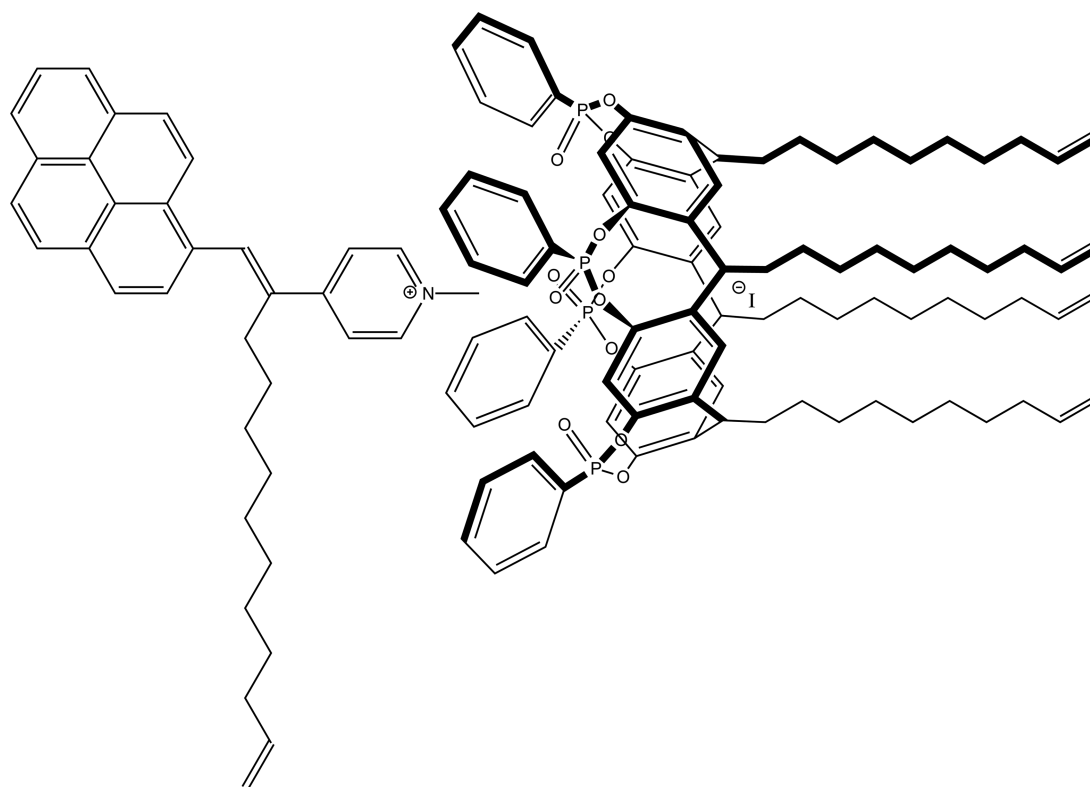


Figure 2. Reporting system, consisting of an *N*-methylated pyridinium salt (guest, left) and a tetraphosphonate cavitand (host, right), held together by specific host–guest interactions.

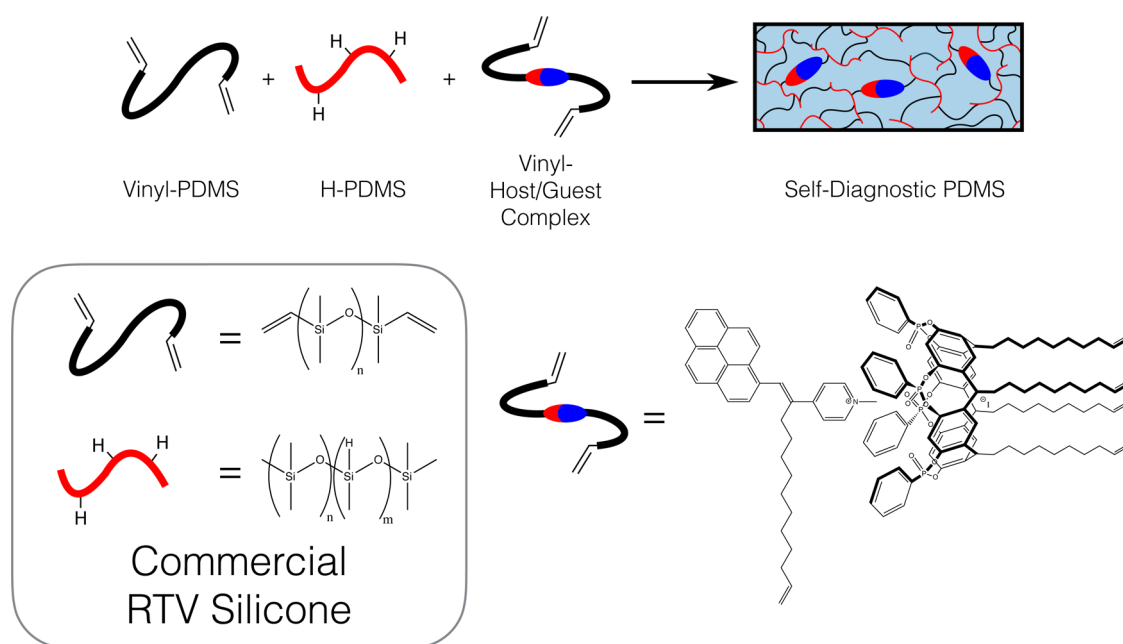


Figure 3. Schematic sketch of the self-diagnostic polymer system (top) and the respective chemical structures of the components (bottom).

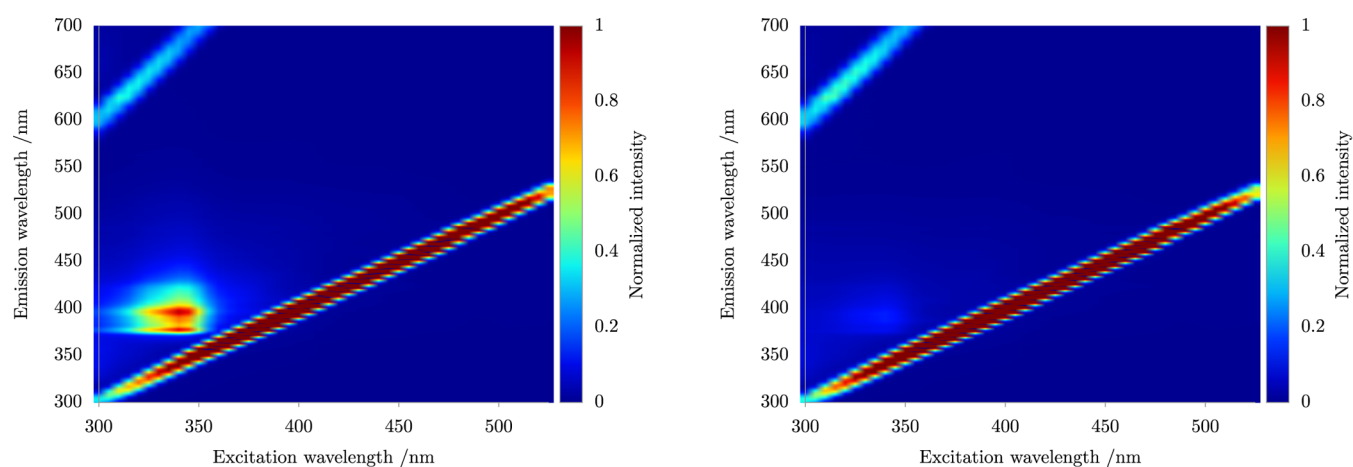


Figure 4. Steady-state fluorescence spectra of free guest (left) and the complex in PDMS (right). Both samples contain the guest in a concentration of $b = 10^{-6} \text{ mol kg}^{-1}$. The two lines are caused by first and second order Rayleigh scattering.

265 and the guest are then mixed together in dichloromethane
 266 (DCM) solution in a 2:1 ratio to form the desired complex.
 267 This solution is added to the vinyl-PDMS component, and the
 268 residual DCM is removed by heating, giving a homogeneous
 269 mixture. Then the H-PDMS and the catalyst are added to the
 270 mixture, homogenized, and poured into cuvettes for fluorescent
 271 measurements or in molds for mechanical tests. The curing is
 272 performed directly into cuvettes and molds by heating them in
 273 the oven to 40 °C overnight.

274 **Fluorescence Characterization.** The reporting complex is
 275 designed in a way that its dissociation leads to fluorescence
 276 emission. The *N*-methylated pyridinium salt itself, consisting of
 277 a pyrene conjugated with the pyridinium system, is highly
 278 fluorescent in solution as well as in the PDMS polymer matrix
 279 (Figure 4 left). Upon complexation, this fluorescence is
 280 quenched (Figure 4, right). This provides an easy and very
 281 sensitive method of detection for the dissociation of the
 282 complex. In solution, complete complexation of the fluorescent
 283 guest is ensured using a twofold excess of the host.

The fluorescence of the guest was measured in DCM 284
 solution with a concentration of $c(\text{guest}) = 10^{-6} \text{ M}$ as well as in 285
 PDMS matrix with a concentration $b(\text{guest}) = 10^{-6} \text{ mol kg}^{-1}$, 286
 both in the presence and absence of the cavitand host (see 287
 Experimental Section and Figures S1 and S2). 288

As clearly visible in Figure 4, the guest alone shows an 289
 intense fluorescence in the PDMS matrix when excited with 290
 ultraviolet light of about $\lambda = 345 \text{ nm}$ with maximum emissions 291
 at $\lambda = 380 \text{ nm}$ and $\lambda = 400 \text{ nm}$. In the complexed state, the 292
 fluorescence emission is almost completely quenched. Un- 293
 functionalized PDMS as well as PDMS containing only the host 294
 show no fluorescence emission in the measured range (see 295
 Figure S2). 296

Mechanical Testing and Theoretical Analysis. The 297
 proposed complex, uniformly and isotropically distributed in 298
 the polymer matrix, can provide information related to the 299
 volumetric strain state in the material upon detachment. Thus, 300
 when mechanical stress is applied to the system, it is expected 301

302 that the complex will be separated before any damage is done
303 to the material.

304 **Preliminary Tests.** To test the performances of the
305 reporting probe, specimens containing 10^{-6} mol kg^{-1} of the
306 host–guest complex were prepared (Figure 5). The tiny

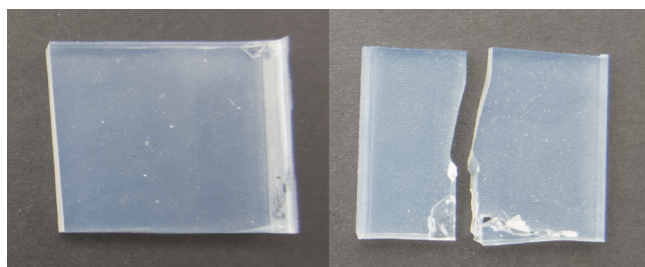


Figure 5. PDMS samples before and after breaking.

307 amount of reporting complex added does not alter the color or
308 transparency of the samples. These specimens were investigated
309 under the fluorescence microscope and subsequently first
310 stretched and then broken. After every step, the fluorescence of
311 each sample was reassessed. As shown in Figure 6, the samples

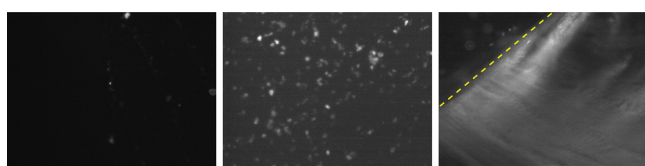


Figure 6. Fluorescence images of the sample before stretching (left), after stretching (middle), and after breaking (right). The dashed yellow line indicates the breaking edge.

312 exhibit no fluorescence in the pristine state (left). However,
313 after stretching, clearly detectable fluorescence features appear
314 (middle), which were even more prominent after breaking the
315 sample and the most intense along the breaking edge (right).
316 Interestingly, most of the fluorescence is not observed at the
317 fracture edge but in the nearby stressed region. On the basis of
318 those findings, it was decided to investigate the fluorescence
319 emission both theoretically and experimentally.

320 **Mechanical Characterization.** PDMS specimens, with
321 and without self-diagnostic complexes, have been characterized
322 (Table 1). Because of the chosen geometry of the specimen
323 (Figure 7) and the test procedure, the crack grows in a stable
324 fashion along the middle cross-section of the beam triggered by
325 the initial indentation. The mechanical parameters of the
326 various specimens are almost identical, proving that the
327 addition of the host–guest complex to the matrix does not
328 alter the micromechanical structure of the material. In Table 1
329 the geometrical and mechanical characteristics of the tested
330 specimens are reported. The addition of the host–guest
331 complex to the matrix does not modify the elastic modulus

and the Poisson's ratio of the polymer, which are the two main
mechanical characteristics of material. These are the values,
together with the material's strength, that must fulfill the design
requirements in real applications in order to guarantee the
desired mechanical response to external actions.

For sake of completeness, in Table 1 the geometrical
parameters (length, width W , initial crack depth a_0 , thickness t ,
and curvature radius ρ at the notch tip) characterizing the
precracked beam specimen are also reported (dimensions in
moreover, the energy \mathcal{G}_c necessary for the formation
of the unit area of fracture and the fracture toughness related
parameter, K_{Ic} , are also given for the tested materials. The three
point bending test has been performed on prenotched
specimens, like the one shown in Figure 7b, whose geometry
is typical for producing a progressive opening crack growth in
Mode I.⁴² The loading process has been experimentally
monitored using Digital Image Correlation (DIC) analysis. This
contactless technique enables the kinematics of the
deformation of the material to be measured, without interfering
with the specimens.

Finite Element Analysis. An accurate finite element (FE)
analysis of the specimen has been performed by adopting
material elasticity and geometrical nonlinearity. The material
behavior being roughly linear elastic up to the first crack
growth, a mechanically linear analysis provides the stress and
strain values close to the crack tip.

The experimental load versus displacement curve is
illustrated in Figure 8a. The evolution of the strained zone
extension ahead of the crack tip during the loading process
obtained by the FE analysis is shown Figure 8b–d. The
numerical results, reporting the horizontal Green–Lagrange
strain component E_{xx} refer to the instant before the beginning
of the crack growth for $\delta = 12$ mm, indicated by the arrow in
Figure 8a. The corresponding experimental strain map obtained
through the DIC analysis is shown in Figure 8e. The dashed
lines indicate the profile of the specimen and of the mechanical
part used to impose the downward displacement to the upper
midspan point of the specimen. The indicated square plates are
placed laterally to specimen in order to prevent any possible
out-of-plane displacement, i.e., to avoid displacements in the z -
direction. The correspondence between the experimental and
the numerical strain values is satisfactory. These results indicate
the region of maximum strain in the specimens during the
whole load history, defining spatial region and loading
conditions to expect the self-diagnostic fluorescence emission.

Self-Diagnostic Fluorescence Emission. In Figure 9 the
fluorescence measurements and the relative color map intensity
are shown for the blank specimen 1a (see Table 1) in the area
around the initial crack tip after the crack started to grow, while
in Figure 10 the fluorescence pictures and their color maps are
shown for the specimen 1b (the self-diagnostic specimen 1c
showed similar results). The small fluorescence spots outside
the strained region appearing in Figure 9 are not strain-related
fluorescence but are due to dust or small inclusions embedded

Table 1. Geometrical and Mechanical Characteristics of the Tested Specimens^a

spec. no.	L , mm	W , mm	a_0 , mm	t , mm	ρ , μm	self-diagnostic	E , MPa	ν	g_c , m/N	K_{Ic} (MPa $\sqrt{\text{m}}$)
1a	102	25	5	6	150	no	0.99	0.43	111	16.2
1b	102	25	5	6	150	yes	0.98	0.43	108	16.2
1c	102	25	5	6	150	yes	1.01	0.43	110	16.2

^a E , elastic modulus; ν , Poisson's coefficient; \mathcal{G}_c , fracture energy; K_{Ic} , fracture toughness.

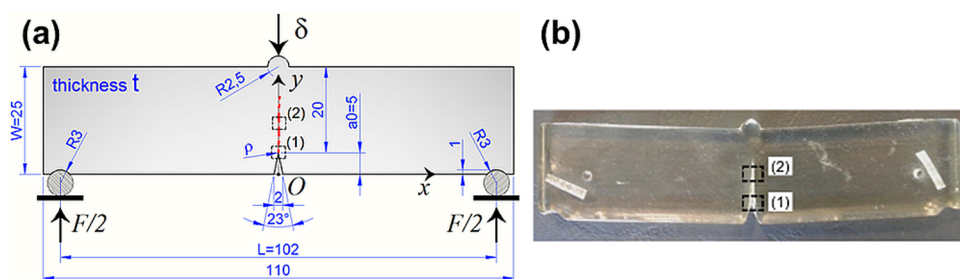


Figure 7. (a) Dimensions of the samples used for three-point bending mechanical stress tests (all lengths are given in millimeters). (b) Side view of the specimen after the propagation of the initial crack (after test finish). Locations (1) and (2) where the fluorescence picture have been taken are shown.

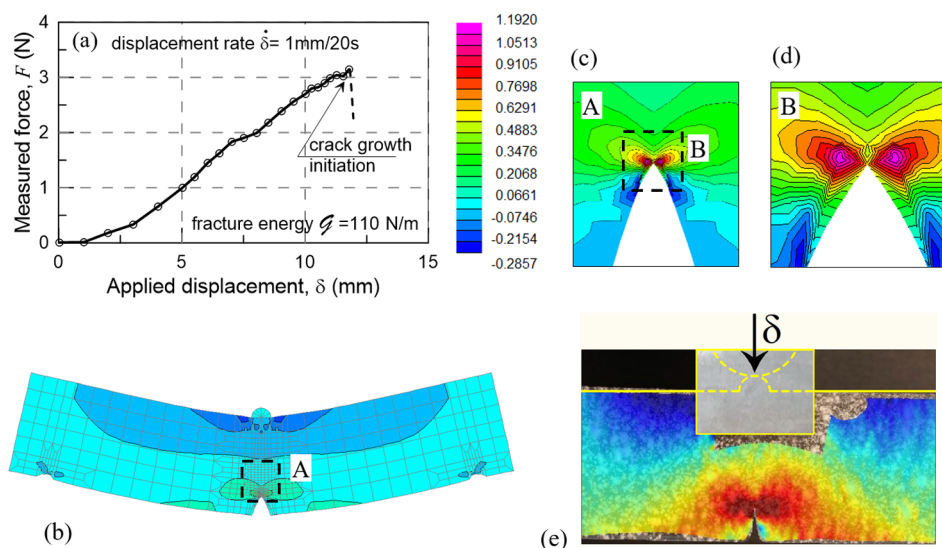


Figure 8. Experimental load–displacement curve for the specimen 1b (a). Map of the strain E_{xx} in the deformed beam obtained through the FE analysis (b), related details (c, d), and experimental DIC analysis results (e) of the crack tip region for an applied downward displacement $\delta = 12$ mm (the Green–Lagrange deformation is displayed in the initial undeformed specimen configuration).

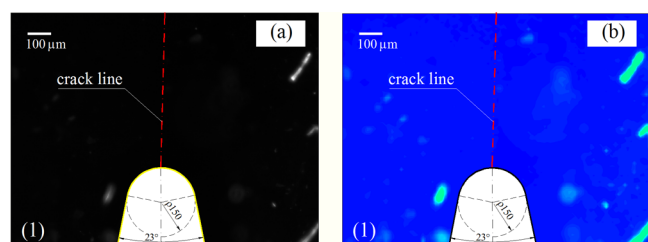


Figure 9. (a) Fluorescence image of the crack tip region (1) (see Figures 7a and 10) for the blank specimen 1a. Color map and related normalized intensity scale of the measured fluorescence in the same region (b).

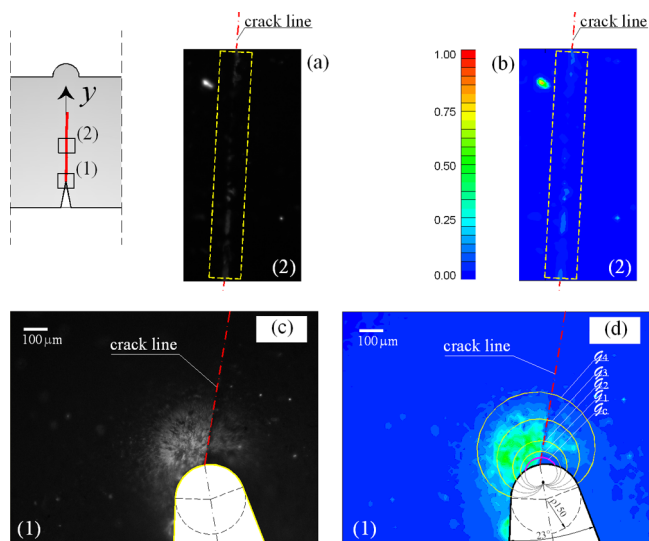


Figure 10. (a) Fluorescence images (a, c) and corresponding normalized fluorescence color maps (b, d) of the crack tip region (1) and along the crack growth path (2). In part d the iso-hydrostatic tensile strain curves, obtained by FE analysis, are also plotted: they correspond to the energy values $\mathcal{G}_c = 110$ N/m (critical energy for material failure) and $\mathcal{G}_1 = 83$ N/m, $\mathcal{G}_2 = 55$ N/m, $\mathcal{G}_3 = 27$ N/m, and $\mathcal{G}_4 = 11$ N/m.

386 in the material that provide a false brightness in the pictures
387 taken under UV light.

388 Both the initial notch tip region (1) (Figure 10c,d) and the
389 area along the crack path (2) (Figure 10a,b) have been
390 considered; it can be clearly noted that the fluorescence appears
391 in highly stretched regions. In particular, the stretched area
392 around the initial crack tip shows the highest fluorescence
393 evidence, due to the localized strain arising before the crack
394 growth. This is in accordance to the numerical model and DIC
395 analysis shown in a previous section.

396 The highest strained region (located at the crack tip) has a
397 very small size compared to the crack, and therefore only a tiny

398 narrow trace of the propagating straight defect can be
399 appreciated in Figure 10a,b.

400 A proper strain-related quantity needs to be assumed to
401 correlate the fluorescence regions of the stretched specimen to
402 the mechanical deformation. As explained in the Supporting
403 Information, a damage-related parameter can be defined
404 according to the so-called cavitation criterion^{27,43} that considers
405 as the primary cause of damage the tensile hydrostatic stress
406 exceeding a certain critical value. The hydrostatic strain
407 represents the mean value, calculated over the normal strains
408 acting in all directions, in a given point of the material. Since
409 the host–guest complex is isotropically oriented inside the
410 polymeric matrix, the number of separated hosts and guests is
411 proportional to the mean strain. It is therefore reasonable to
412 assume that the observed fluorescence intensity provides a
413 measure of the mean strain value.

414 In Figure 10d the iso-hydrostatic strain curves are displayed
415 (see yellow lines) for different values of the energy ($\mathcal{G}_c > \mathcal{G}_1 >$
 $\mathcal{G}_2 > \mathcal{G}_3 > \mathcal{G}_4$, see Supporting Information); in particular the
416 smallest region identified by the pink curve corresponds to the
417 critical energy \mathcal{G}_c (see Table 1) that identifies the damaged
418 region of the material produced by the applied mechanical
419 stress. Outside the curve corresponding to the critical energy
 \mathcal{G}_c , the material is still elastic and recovers completely its initial
420 free-strain state after unloading. However, the cavitation-based
421 sensing system provides a clear trace of the strains previously
422 occurred in the material. It is worth noting that the fluorescence
423 picture and the corresponding map show a certain asymmetry
424 with respect to the crack axis. This can be explained by
425 considering that the crack does not grow along the symmetry
426 axis of the specimen, so the strain field as a result is asymmetric.

427 ■ CONCLUSIONS

428 In conclusion, we prepared and characterized a self-diagnostic
429 PDMS polymer, exploiting the fluorescence properties of a
430 pyrene conjugated *N*-methylpyridinium salt guest in combina-
431 tion with a tetrakisphosphate cavitand host. The polymer
432 exhibits no fluorescence when the intact complex is present but
433 a clear fluorescence emission of the guest when dissociated
434 from the host. In this way, it is possible to detect regions of
435 high volumetric strain intensity. The fluorescence maps
436 obtained from a mechanically tested, cracked sample compared
437 with the strain results from numerical analysis and DIC
438 measurements showed a good correlation. We therefore believe
439 that the presented system is suitable for the detection of regions
440 of high volumetric strain in soft polymeric matrices and thus
441 can be used to predict the failure of such materials, increasing
442 their applicability, reliability, and safety level, especially with
443 regard to the in-service maintenance planning. Further, it can
444 be relevant to observe that such a self-sensing strain system can
445 be easily applicable to any structural element by simply coating
446 it with a thin film of the polymer charged with the host–guest
447 cavitand system. If the base material and the coating one adhere
448 perfectly under the application of the mechanical loading, the
449 self-diagnostic layer provides a direct and simple way of
450 quantitatively detecting the strain values in the element
451 underneath.

■ ASSOCIATED CONTENT

■ Supporting Information

The Supporting Information is available free of charge on the
ACS Publications website at DOI: 10.1021/acs.chemma-
ter.7b02438.

Fluorescence characterizations and quantitative modeling
(PDF)

■ AUTHOR INFORMATION

Corresponding Authors

*(R.B.) E-mail: roberto.brighenti@unipr.it.

*(E.D.) E-mail: enrico.dalcanale@unipr.it.

ORCID

Enrico Dalcanale: 0000-0001-6964-788X

Author Contributions

All authors have given approval to the final version of the
manuscript.

Funding

This work is supported by the Hierarchical Self Assembly of
Polymeric Soft Systems (SASSYPOL-ITN) Marie Skłodowska
Curie network, funded through the European Union Seventh
Framework Programme (FP7-PEOPLE-2013-ITN) under
Grant Agreement No. 607602.

Notes

The authors declare no competing financial interest.

■ ACKNOWLEDGMENTS

We thank Davide Orsi for assistance with the fluorescence
microscope.

■ ABBREVIATIONS

DCM, dichloromethane; DIC, digital image correlation; EtOAc, ethyl acetate; FE, finite element; Hex, hexane; PDMS, poly(dimethylsiloxane); SWCNT, single-walled carbon nanotube; THF, tetrahydrofuran; UV, ultraviolet

■ REFERENCES

- (1) Clough, J. M.; Balan, A.; Sijbesma, R. P. Mechanochemical Reactions Reporting and Repairing Bond Scission in Polymers. *Top. Curr. Chem.* **2015**, *369*, 209–238.
- (2) Black, A. L.; Lenhardt, J. M.; Craig, S. L. From molecular mechanochemistry to stress-responsive materials. *J. Mater. Chem.* **2011**, *21*, 1655–1663.
- (3) Li, J.; Nagamani, C.; Moore, J. S. Polymer Mechanochemistry: From Destructive to Productive. *Acc. Chem. Res.* **2015**, *48*, 2181–2190.
- (4) Pucci, A.; Bizzarri, R.; Ruggeri, G. Polymer composites with smart optical properties. *Soft Matter* **2011**, *7*, 3689–3700.
- (5) Ciardelli, F.; Ruggeri, G.; Pucci, A. Dye-containing polymers: methods for preparation of mechanochromic materials. *Chem. Soc. Rev.* **2013**, *42*, 857–870.
- (6) Lee, C. K.; Davis, D. A.; White, S. R.; Moore, J. S.; Sottos, N. R.; Braun, P. V. Force-Induced Redistribution of a Chemical Equilibrium. *J. Am. Chem. Soc.* **2010**, *132*, 16107–16111.
- (7) Marelli, B.; Patel, N.; Duggan, T.; Perotto, G.; Shirman, E.; Li, C.; Kaplan, D. L.; Omenetto, F. G. Programming function into mechanical forms by directed assembly of silk bulk materials. *Proc. Natl. Acad. Sci. U. S. A.* **2017**, *114*, 451–456.
- (8) O'Bryan, G.; Wong, B. M.; McElhanon, J. R. Stress Sensing in Polycaprolactone Films via an Embedded Photochromic Compound. *ACS Appl. Mater. Interfaces* **2010**, *2*, 1594–1600.
- (9) Davis, D. A.; Hamilton, A.; Yang, J.; Cremer, L. D.; Van Gough, S. D.; Potisek, S. L.; Ong, M. T.; Braun, P. V.; Martinez, T. J.; White, S. 509 R.; Moore, J. S.; Sottos, N. R. Force-induced activation of covalent

- 511 bonds in mechanoresponsive polymeric materials. *Nature* **2009**, *459*,
512 68–72.
- 513 (10) Klajn, R. Spiropyran-based dynamic materials. *Chem. Soc. Rev.*
514 **2014**, *43*, 148–184.
- 515 (11) Chen, Y.; Spiering, A. J. H.; Karthikeyan, S.; Peters, G. W. M.;
516 Meijer, E. W.; Sijbesma, R. P. Mechanically induced chemilumines-
517 cence from polymers incorporating a 1,2-dioxetane unit in the main
518 chain. *Nat. Chem.* **2012**, *4*, 559–562.
- 519 (12) Ducrot, E.; Chen, Y.; Bulters, M.; Sijbesma, R. P.; Creton, C.
520 Toughening Elastomers with Sacrificial Bonds and Watching Them
521 Break. *Science* **2014**, *344*, 186–189.
- 522 (13) Clough, J. M.; Balan, A.; van Daal, T. L. J.; Sijbesma, R. P.
523 Probing Force with Mechanobase-Induced Chemiluminescence.
524 *Angew. Chem., Int. Ed.* **2016**, *55*, 1445–1449.
- 525 (14) Chen, Y.; Sijbesma, R. P. Dioxetanes as Mechanoluminescent
526 Probes in Thermoplastic Elastomers. *Macromolecules* **2014**, *47*, 3797–
527 3805.
- 528 (15) Robb, M. J.; Li, W.; Gergely, R. C. R.; Matthews, C. C.; White,
529 S. R.; Sottos, N. R.; Moore, J. S. A Robust Damage-Reporting Strategy
530 for Polymeric Materials Enabled by Aggregation-Induced Emission.
531 *ACS Cent. Sci.* **2016**, *2*, 598–603.
- 532 (16) Rossi, N. A. A.; Duplock, E. J.; Meegan, J.; Roberts, D. R. T.;
533 Murphy, J. J.; Patel, M.; Holder, S. J. Synthesis and characterization of
534 pyrene-labelled polydimethylsiloxane networks: towards the in situ
535 detection of strain in silicone elastomers. *J. Mater. Chem.* **2009**, *19*,
536 7674–7686.
- 537 (17) Yang, L.; Han, J. Electronic Structure of Deformed Carbon
538 Nanotubes. *Phys. Rev. Lett.* **2000**, *85*, 154–157.
- 539 (18) Leeuw, T. K.; Tsyboulski, D. A.; Nikolaev, P. N.; Bachilo, S. M.
540 S. M.; Arepalli, S.; Weisman, R. B. Strain Measurements on Individual
541 Single-Walled Carbon Nanotubes in a Polymer Host: Structure-
542 Dependent Spectral Shifts and Load Transfer. *Nano Lett.* **2008**, *8*,
543 826–831.
- 544 (19) Zeng, S.; Zhang, D.; Huang, W.; Wang, Z.; Freire, S. G.; Yu, X.;
545 Smith, A. T.; Huang, E. Y.; Nguon, H.; Sun, L. Bio-inspired sensitive
546 and reversible mechanochromisms via strain-dependent cracks and
547 folds. *Nat. Commun.* **2016**, *7*, 11802.
- 548 (20) Zhang, X.; Chi, Z.; Zhang, Y.; Xu, J.; Liu, S. Recent advances in
549 mechanochromic luminescent metal complexes. *J. Mater. Chem. C*
550 **2013**, *1*, 3376–3390.
- 551 (21) Xu, J.; Chi, Z. *Mechanochromic Fluorescent Materials*; Royal
552 Society of Chemistry: Cambridge, U.K., 2014.
- 553 (22) Gossweiler, G. R.; Hewage, G. B.; Soriano, G.; Wang, Q.;
554 Welshofer, G. W.; Zhao, X.; Craig, S. L. Mechanochemical Activation
555 of Covalent Bonds in Polymers with Full and Repeatable Macroscopic
556 Shape Recovery. *ACS Macro Lett.* **2014**, *3*, 216–219.
- 557 (23) Clough, J. M.; Creton, C.; Craig, S. L.; Sijbesma, R. P. Covalent
558 Bond Scission in the Mullins Effect of a Filled Elastomer: Real-Time
559 Visualization with Mechanoluminescence. *Adv. Funct. Mater.* **2016**, *26*,
560 9063–9074.
- 561 (24) Botsis, J.; Humbert, L.; Colpo, F.; Giaccari, P. Embedded fiber
562 Bragg grating sensor for internal strain measurements in polymeric
563 materials. *Opt. Lasers Eng.* **2005**, *43*, 491–510.
- 564 (25) Liehr, S.; Lenke, P.; Wendt, M.; Krebber, K.; Seeger, M.; Thiele,
565 E.; Metschies, H.; Gebreselassie, B.; Munich, J. C. Polymer Optical
566 Fiber Sensors for Distributed Strain Measurement and Application in
567 Structural Health Monitoring. *IEEE Sens. J.* **2009**, *9*, 1330–1338.
- 568 (26) Boyce, M. C.; Arruda, E. M. Constitutive Models of Rubber
569 Elasticity: A Review. *Rubber Chem. Technol.* **2000**, *73*, 504–523.
- 570 (27) Fond, C. Cavitation criterion for rubber materials: A review of
571 void-growth models. *J. Polym. Sci., Part B: Polym. Phys.* **2001**, *39*,
572 2081–2096.
- 573 (28) Rondeau, R. E. Slush Baths. *J. Chem. Eng. Data* **1966**, *11*, 124.
- 574 (29) Misztal, K.; Tudisco, C.; Sartori, A.; Malicka, J. M.; Castelli, R.;
575 Condorelli, G. G.; Dalcanale, E. Hierarchical Self-Assembly of
576 Luminescent Eu^{III} Complexes on Silicon. *Eur. J. Inorg. Chem.* **2014**,
577 *2014*, 2687–2694.
- 578 (30) Bibal, B.; Tinant, B.; Declercq, J.-P.; Dutasta, J.-P. Preparation
579 and Structure of [iiiii] Tetraphosphonatocavitands Bearing Long
Chain Functionality at the Lower Rim: Metal Picrates Extraction
Studies. *Supramol. Chem.* **2003**, *15*, 25–32. 580
581
- (31) PerkinElmer. *FL WinLab*; 2001. 582
- (32) Williams, T.; Kelley, C. *gnuplot*; 2016. 583
- (33) Blaber, J.; Adair, B.; Antoniou, A. Ncorr: Open-Source 2D 584
Digital Image Correlation Matlab Software. *Exp. Mech.* **2015**, *55*, 585
1105–1122. 586
- (34) Blaber, J.; Antoniou, A. *DIC Algorithms*. 587
- (35) Schneider, C. A.; Rasband, W. S.; Eliceiri, K. W. NIH Image to 588
ImageJ: 25 years of image analysis. *Nat. Methods* **2012**, *9*, 671–675. 589
- (36) Yebeutchou, R. M.; Tancini, F.; Demitri, N.; Geremia, S.; 590
Mendichi, R.; Dalcanale, E. Host–Guest Driven Self-Assembly of 591
Linear and Star Supramolecular Polymers. *Angew. Chem., Int. Ed.* **2008**, 592
47, 4504–4508; *Angew. Chem.* **2008**, *120*, 4580–4584. 593
- (37) Pinalli, R.; Brancatelli, G.; Pedrini, A.; Menozzi, D.; Hernandez, 594
D.; Ballester, P.; Geremia, S.; Dalcanale, E. The Origin of Selectivity in 595
the Complexation of *N*-Methyl Amino Acids by Tetrphosphonate 596
Cavitands. *J. Am. Chem. Soc.* **2016**, *138*, 8569–8580. 597
- (38) Menozzi, D.; Biavardi, E.; Massera, C.; Schmidtchen, F.-P.; 598
Cornia, A.; Dalcanale, E. Thermodynamics of host–guest interactions 599
between methylpyridinium salts and phosphonate cavitands. *Supramol.* 600
Chem. **2010**, *22*, 768–775. 601
- (39) Pinalli, R.; Dalcanale, E. Supramolecular Sensing with 602
Phosphonate Cavitands. *Acc. Chem. Res.* **2013**, *46*, 399–411. 603
- (40) Koh, K. N.; Araki, K.; Ikeda, A.; Otsuka, H.; Shinkai, S. Shinkai, 604
Reinvestigation of Calixarene-Based Artificial-Signaling Acetylcholine 605
Receptors Useful in Neutral Aqueous (Water/Methanol) Solution. S. 606
J. Am. Chem. Soc. **1996**, *118*, 755–758. 607
- (41) Moretto, H.-H.; Schulze, M.; Wagner, G. Silicone. *Ullmann's* 608
Encyclopedia of Industrial Chemistry; Wiley-VCH: Weinheim, Germany, 609
2000. 610
- (42) Kanninen, M. F.; Popelar, C. H. Advanced fracture mechanics. 611
Oxford Engineering Science series; Oxford University Press: Oxford, 612
U.K., 1985. 613
- (43) Lin, Y. Y.; Hui, C. Y. Cavity growth from crack-like defects in 614
soft materials. *Int. J. Fract.* **2004**, *126*, 205–221. 615